

Spin-orbit-coupled spin-1 Bose-Einstein condensates in a toroidal trap: even-petal-number necklacelike state and persistent flow

Keyan Liu, Huaxin He, Chenhui Wang, Yuanyuan Chen, and Yongping Zhang*
International Center of Quantum Artificial Intelligence for Science and Technology (QuArtist) and Department of Physics, Shanghai University, Shanghai 200444, China

Spin-orbit coupling has novel spin-flip symmetries, a spin-1 spinor Bose-Einstein condensate owns meaningful interactions, and a toroidal trap is topologically nontrivial. We incorporate the three together and study the ground-state phase diagram in a Rashba spin-orbit-coupled spin-1 Bose-Einstein condensate with a toroidal trap. The spin-flip symmetries give rise to two different interesting phases: persistent flows with a unit phase winding difference between three components, and necklace states with even petal-number. The existing parameter regimes and properties of these phases are characterized by two-dimension numerical calculations and an azimuthal analytical one-dimension model.

I. INTRODUCTION

In atomic Bose-Einstein condensates (BECs), confinements play a key role in variously pertinent physics. One of the salient confining geometries is toroidal trap. Considering macroscopic quantum property of BECs, periodic boundary imposed by toroidal trap naturally gives rise to atomic persistent flows [1]. Since preparations of ring-shaped trap can be implemented precisely in experiments [1, 2], BECs in a toroidal trap become a prototypical system to investigate superfluidity [3–8]. Furthermore, such confinement can be easily equipped with rotation created by rotating repulsive perturbation [9]. The response of superfluids to rotation in a toroidal trap has been widely investigated [9–17].

The generalization of single-component toroidal BECs to multicomponents also draws much attention [18]. The population imbalance and fixed phase relation between multiple components bring persistent flows novel stability features [18–22]. It has been found that rich phase diagram and interesting collective excitations can exist in interacting two-component [23–26] and three-component [27–29] toroidal BECs.

Each component behaves as a pseudo-spin state, therefore, two components correspond to spin-1/2 and three components can be explained as spin-1. Pseudo-spins can be arranged to couple with external momentum, which leads to so called spin-orbit coupling. It must be introduced into multi-component BECs artificially [30]. Experimental realizations of spin-orbit-coupled BECs represent current advances in ultracold atomic physics [31–33]. The striking feature of spin-orbit-coupled BECs is the spontaneous emergence of striped density patterns as ground states [34–39]. They are due to Bosons condense simultaneously into multiple energy-minimum states, as distinct from conventional condensations that condense into only one energy minimum. Putting spin-orbit-coupled BECs in a toroidal trap quickly attracts interests [40–46]. Phase diagram of spin-orbit-coupled spin-

1/2 BECs in a tight toroidal trap has been identified [41–43]. The non-trivial topology of the toroidal trap generates new features to striped patterns for Raman-induced spin-orbit coupling [41]. While Rashba spin-orbit coupling has same rotating symmetry as the toroidal trap, density modulation for Rashba case is patterned along azimuthal direction appearing as a necklace [42, 43]. The most interesting is such a necklacelike state has an odd number of petals [43]. It is also revealed that in Rashba spin-1/2 BECs both two components can support persistent flows with a unit winding number difference between them [43]. Spin-orbit-coupled spin-1 BECs support more enriching phases. The effort in existing studies on spin-1 has been put into investigating the interplay between spin-orbit coupling and rotation [44–46]. The characteristics of phase diagram for spin-orbit-coupled spin-1 BECs with a toroidal confinement are still lacking. Considering the existence of the odd-petal-number necklace state in spin-1/2 system, it is natural to ask whether the necklace state still has specific petal-number and what the persistent flow is in spin-1 BECs.

In this paper, we systematically characterize the ground-state phase diagram of a Rashba spin-orbit-coupled spin-1 BEC in a two dimensional toroidal trap. The phases are identified from both direct numerical calculations and an analytical study for a tight trap. When the toroidal trap is tight, the dynamics along radial direction can be frozen, two dimensional system is reduced to an one-dimension effective model only considering the dynamics along azimuthal direction. The effective model provides an analytical means to qualitatively understand two dimensional numerical results. A spin-1 spinor BEC features density-density interaction and spin-spin interaction with respective strength c_0 and c_2 [47]. For an antiferromagnetic interaction $c_2 > 0$, depending on the spin-orbit coupling strength, there are two phases: persistent flows with the winding number $(-1, 0, 1)$ for three components and necklace states with even petal-number. For a ferromagnetic interaction $c_2 < 0$, the ground state is a persistent flow, and there is always a unit winding number difference between three components. We find that the origination and properties of all phases relate to

* yongping11@t.shu.edu.cn

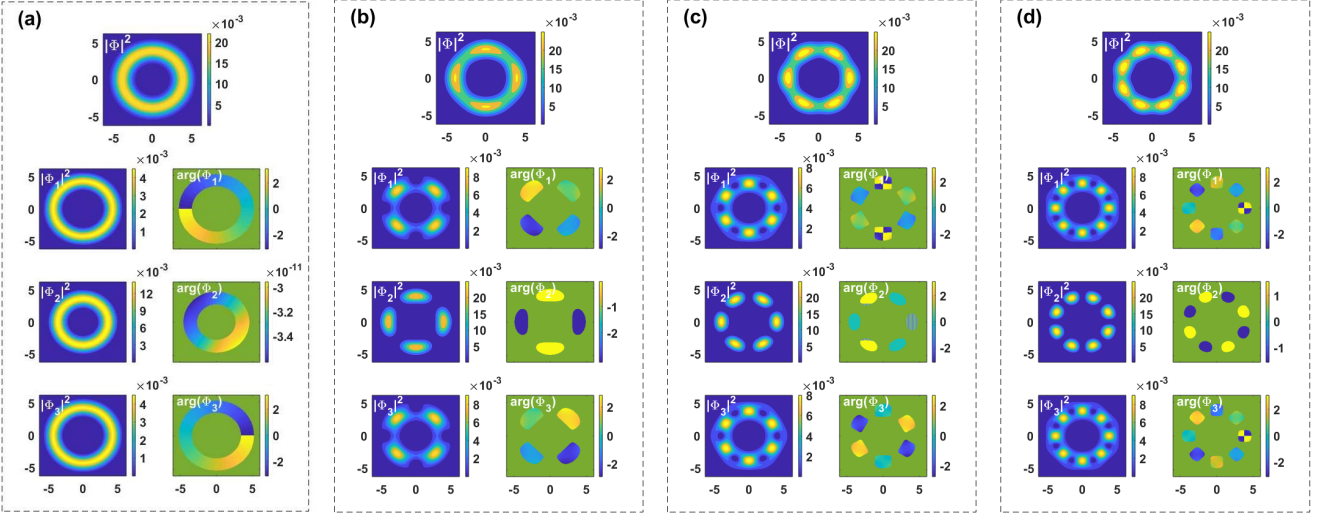


FIG. 1. Ground states with the antiferromagnetic interaction $c_2 = 1$ for different spin-orbit coupling strength λ . (a) $\lambda = 0.4$, (b) $\lambda = 0.6$, (c) $\lambda = 1.0$, (d) $\lambda = 1.2$. Other parameters are $r_0 = 0.4$ and $c_0 = 10$. In each block, the top panel is the total density distribution $|\Phi|^2 = |\Phi_1|^2 + |\Phi_2|^2 + |\Phi_3|^2$, followed by density distribution of each component on the left and corresponding phase distribution of each component on the right.

extraordinary spin-flip symmetries.

This paper is organized as follows. In Sec. II, we present the phase diagram from two dimensional numerical calculations. Features of the persistent flow and necklace state are addressed by a spin-flip symmetry. In Sec. III, we develop an one-dimension analytical model to capture physics along the azimuthal direction. From the model, all phases are identified using a variational wave function. A clear physical picture is provided for the existence and properties of ground state. Especially we address why the necklace state must have even petal-number in a spin-1 BEC, while it would have odd number in a spin-1/2 analog. Sec. IV is the conclusion.

II. PHASE DIAGRAM

The experimental realization of Raman-induced spin-orbit coupling in a spin-1 BEC [48] stimulates to explore spin-orbit-coupled spinor BECs. Ground states and collective excitations of a homogeneously spin-orbit-coupled spin-1 BEC have been investigated theoretically [49–53]. With a toroidal trap, the system is described by the Gross-Pitaevskii equation (GPE) [44, 52],

$$i\hbar \frac{\partial \Phi}{\partial t} = (H_{\text{sin}} + H_{\text{int}}) \Phi. \quad (1)$$

The spinor wave function $\Phi = (\Phi_1, \Phi_2, \Phi_3)^T$ describes the occupation of three components. The single-particle Hamiltonian in Eq. (1) is

$$H_{\text{sin}} = \frac{p_x^2 + p_y^2}{2m} + \lambda(F_x p_y - F_y p_x) + V(r), \quad (2)$$

with m being the mass of the atom. p_x and p_y are momenta along x and y directions respectively. (F_x, F_y, F_z)

are spin-1 Pauli matrices. The Rashba spin-orbit coupling is $\lambda(F_x p_y - F_y p_x)$ with the coupling strength λ . The external trap is two dimensional toroidal, $V(r) = \frac{1}{2}m\omega_r^2(r - r_0)^2$, here $r^2 = x^2 + y^2$, the radius of torus is r_0 , and ω_r is the trapping frequency. In the GPE, the nonlinear part is

$$H_{\text{int}} = \begin{pmatrix} c_0\rho_0 + c_2\rho_z & c_2\rho_2 & 0 \\ c_2\rho_2^* & c_0\rho_0 & c_2\rho_2 \\ 0 & c_2\rho_2^* & c_0\rho_0 - c_2\rho_z \end{pmatrix}, \quad (3)$$

where $\rho_0 = |\Phi_1|^2 + |\Phi_2|^2 + |\Phi_3|^2$, $\rho_z = |\Phi_1|^2 - |\Phi_3|^2$, and $\rho_2 = \Phi_2^*\Phi_1 + \Phi_3^*\Phi_2$. The nonlinearity is characterized by the density-density interaction with the coefficient c_0 and spin-spin interaction with the coefficient c_2 . We numerically solve the GPE by the imaginary time evolution method to get ground states. In detail calculations, we use the dimensionless GPE by scaling the energy, length, time and λ in units of $\hbar\omega_r$, $\sqrt{\hbar/m\omega_r}$, $1/\omega_r$ and $\sqrt{\hbar\omega_r/m}$ respectively. The wave function satisfies normalization condition, $\int dx dy (|\Phi_1|^2 + |\Phi_2|^2 + |\Phi_3|^2) = 1$.

Typical ground states for an antiferromagnetic interaction $c_2 > 0$ with different spin-orbit coupling strength λ are demonstrated in Fig. 1. There are two different phases. (1) When λ is small, three components distribute homogeneously in the ring [see Fig. 1(a)]. The first and third components share the same density, $|\Phi_1|^2 = |\Phi_3|^2$, and have an opposite-sign phase winding ± 1 . These two components support persistent flows with a unit phase winding. While, there is no phase winding in the second component. The existence of phase winding makes the size of the first and third components is larger than that of the second component. (2) When λ is relatively large, the ground state becomes necklacelike patterns, which are shown in Fig. 1(b-d). Three components have a same

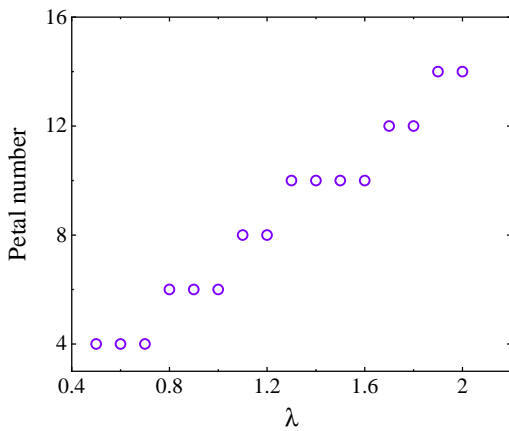


FIG. 2. The number of petals in the necklace state as a function of the spin-orbit coupling strength λ . It is found that the petal-number is always even. The other parameters are same as in Fig. 1.

petal-number. The density of the first component is same as that of the third component, $|\Phi_1|^2 = |\Phi_3|^2$. The petals in the second component don't spatially overlap with these in Φ_1 and Φ_3 . The total density also shows a neck-lacelike geometry. These states are reminiscent of stripe phases from a homogeneous spin-orbit-coupled BEC. In homogeneous system, Rashba spin-orbit coupling can induce density stripes whose orientation is spontaneously chosen [34, 37]. In the toroidal trap, the stripes are oriented along the azimuthal direction. Via this way, the boundaries of each petal in the necklace can be shortened for minimizing kinetic energy. The petal-number increases as a function of λ . In Fig. 2, we show the dependence of petal-number on λ , and find that the petal-number is always even and increases almost linearly with λ . The even-petal-number necklace state in spin-1 BECs is strikingly different from the only existed odd-number analog in spin-1/2 [43]. It is noting that only necklace states with four times number of petals are numerically found in Ref. [44].

These two different ground states have two common features. From density and phase distributions in Fig. 1, we know that two ground states obey a same spin-flip symmetry \hat{O} ,

$$\hat{O} = \mathcal{K}e^{i\pi F_y} = \mathcal{K} \begin{pmatrix} 0 & 0 & 1 \\ 0 & -1 & 0 \\ 1 & 0 & 0 \end{pmatrix}. \quad (4)$$

Here, \mathcal{K} is the complex conjugate operator, and $e^{i\pi F_y}$ is the operator to rotate spins by the angle of π along the F_y axis. The GPE and single-particle Hamiltonian H_{sin} have the symmetry \hat{O} . Ground states inherit the symmetry and are its eigenstates with eigenvalue ± 1 . This gives rise to $\Phi_1 = \pm\Phi_3^*$ and $\Phi_2 = \mp\Phi_2^*$. Therefore, the first and third components have a same density and the wave function of the second component is purely real or imaginary. The other common feature is the phase separation

between Φ_2 and Φ_1, Φ_3 . The nonlinear part of the energy functional corresponding to the GPE is $E_{\text{non}} = E_{\text{dd}} + E_{\text{ss}}$. $E_{\text{dd}} = c_0/2 \int dx dy (|\Phi_1|^2 + |\Phi_2|^2 + |\Phi_3|^2)^2$ is the density-density interaction energy, and the spin-spin interaction energy is $E_{\text{ss}} = c_2/2 \int dx dy [(\Phi^\dagger F_x \Phi)^2 + (\Phi^\dagger F_y \Phi)^2 + (\Phi^\dagger F_z \Phi)^2] = c_2/2 \int dx dy [(|\Phi_1|^2 - |\Phi_3|^2)^2 + 2|\Phi_1|^2|\Phi_2|^2 + 2|\Phi_2|^2|\Phi_3|^2 + \Phi_1\Phi_3\Phi_2^{*2} + \Phi_1^*\Phi_3^*\Phi_2^2]$. Substituting the symmetry result $\Phi_1 = \pm\Phi_3^*$ and $\Phi_2 = \mp\Phi_2^*$ into the energy functional, we immediately realize that ground states having the symmetry \hat{O} minimize the spin-spin interaction, i.e., $E_{\text{ss}} = 0$. The density-density part becomes $E_{\text{dd}} = c_0/2 \int dx dy (4|\Phi_1|^4 + |\Phi_2|^4 + 4|\Phi_1|^2|\Phi_2|^2)$, which is similar to a binary BEC. According to the phase separation condition of the binary BEC, E_{dd} belongs to immiscible interactions, so Φ_1 and Φ_2 must be phase separated. For persistent flow states [as shown in Fig. 1(a)], Φ_2 and Φ_1, Φ_3 are spatially separated in the radial direction. While for necklace states, the separation is along the azimuthal direction.

The above is the ground state with an antiferromagnetic interaction, we find that for a ferromagnetic interaction $c_2 < 0$, it becomes different. Typical results with $c_2 = -1$ and different spin-orbit coupling strength λ are depicted in Fig. 3. The ground state always supports persistent flows and density distributes homogeneously along the radial direction. Every component carries nonzero phase winding. The interesting is that there is always a unit phase winding difference between three components, which can be seen from the number of phase jumps in phase distributions in Fig. 3. The phase winding difference is also demonstrated from the size of density. For fixed parameters, the persistent flow with a large number of phase winding has a larger density size. In Fig. 3(a), for a small λ , the winding number for Φ_1, Φ_2 and Φ_3 are $-3, -2,$ and -1 respectively, and the density size decreases. Increasing the spin-orbit coupling strength, the phase winding in each component increases as shown in Fig. 3(b-d). The dependence of the winding number in the second component on λ is demonstrated in Fig. 4. The winding number increases almost linearly as a function of λ .

Two dimensional numerical phase diagram shows interesting characteristics. According to antiferromagnetic or ferromagnetic interactions, two different persistent flow states exist, and necklace states have even petal-number. In the following, we develop an one-dimension effective model to provide analytical insights into the existence and unique properties of these states.

III. EFFECTIVE MODEL

All states in the previous reflect that the azimuthal effect plays an important role. We assume the toroidal trap is very tight, i.e., ω_r is a large scale. In this condition, the dynamics along the radial direction is frozen into the ground state of the harmonic trap. After integrating over the radial degree of freedom, the dynamics along the az-

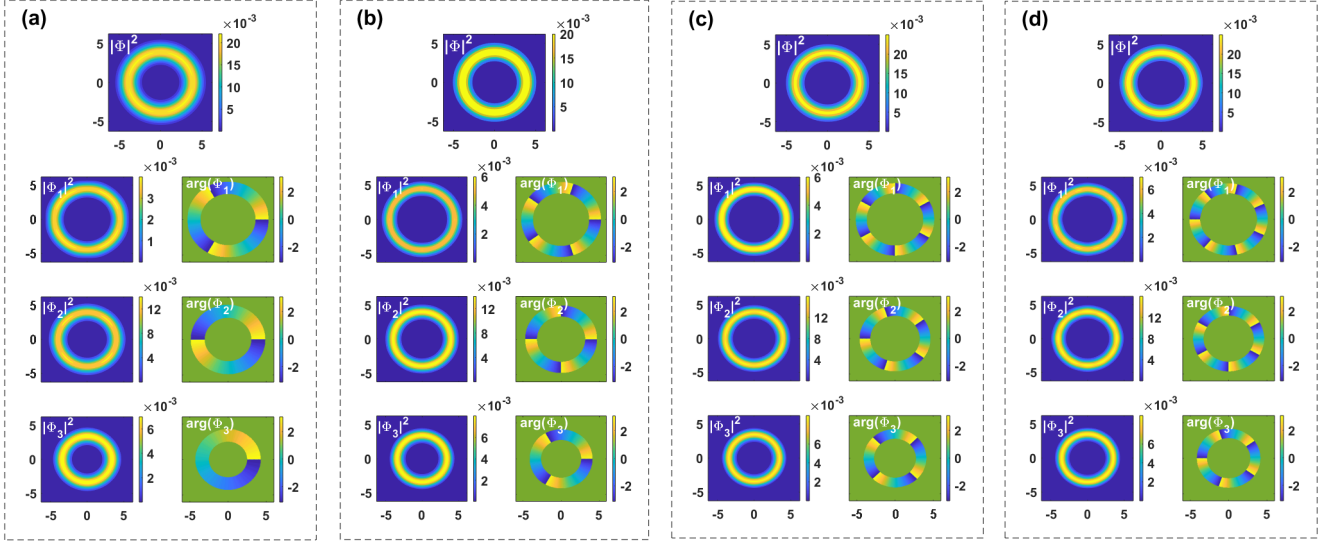


FIG. 3. Ground states with the ferromagnetic interaction $c_2 = -1$ for different spin-orbit coupling strength λ . (a) $\lambda = 0.6$, (b) $\lambda = 1.2$, (c) $\lambda = 1.6$, (d) $\lambda = 1.8$. Other parameters are $r_0 = 0.4$ and $c_0 = 10$. In each block, the top panel is the total density distribution $|\Phi|^2 = |\Phi_1|^2 + |\Phi_2|^2 + |\Phi_3|^2$, followed by density distribution of each component on the left and corresponding phase distribution of each component on the right.

imuthal direction would shine through [40, 43, 54]. The single-particle Hamiltonian in Eq. (2) reduces to one dimensional H_{eff} which effectively describes the azimuthal effect [54],

$$H_{\text{eff}} = \left(-i \frac{\partial}{\partial \phi} \right)^2 + \bar{\lambda} (\cos \phi F_x + \sin \phi F_y) \left(-i \frac{\partial}{\partial \phi} \right) - i \frac{\bar{\lambda}}{2} (\cos \phi F_y - \sin \phi F_x). \quad (5)$$

Here, ϕ is the azimuthal coordinate. H_{eff} is dimensionless, we use the unit of energy as $\hbar^2/(2mr_0^2)$, and $\bar{\lambda} = 2mr_0\lambda/\hbar$. After considering the nonlinear part in Eq. (3), the total energy becomes,

$$E_{\text{tot}} = \frac{1}{2\pi} \int_0^{2\pi} d\phi (\bar{\Phi}^\dagger H_{\text{eff}} \bar{\Phi}) + \frac{\bar{c}_0}{4\pi} \int_0^{2\pi} d\phi |\bar{\Phi}|^4 + \frac{\bar{c}_2}{4\pi} \int_0^{2\pi} d\phi \left[(\bar{\Phi}^\dagger F_x \bar{\Phi})^2 + (\bar{\Phi}^\dagger F_y \bar{\Phi})^2 + (\bar{\Phi}^\dagger F_z \bar{\Phi})^2 \right]. \quad (6)$$

Here, $\bar{c}_0 = 2mr_0^2/\hbar^2 \sqrt{m\omega_r/(2\pi\hbar)} c_0$ and $\bar{c}_2 = 2mr_0^2/\hbar^2 \sqrt{m\omega_r/(2\pi\hbar)} c_2$. The reduced wave function is $\bar{\Phi}(\phi) = (\bar{\Phi}_1(\phi), \bar{\Phi}_2(\phi), \bar{\Phi}_3(\phi))^T$, and $|\bar{\Phi}|^2 = |\bar{\Phi}_1|^2 + |\bar{\Phi}_2|^2 + |\bar{\Phi}_3|^2$.

The effective Hamiltonian H_{eff} conserves J_z with its definition being

$$J_z = -i \frac{\partial}{\partial \phi} + F_z, \quad (7)$$

i.e., $[J_z, H_{\text{eff}}] = 0$. The conservation makes H_{eff} invariant under a rotation $U = \exp(i\theta J_z)$, where θ is an arbitrary angle. Therefore, H_{eff} and U have same eigenstates,

which can be constructed from U as,

$$\bar{\Phi} = e^{in\phi} \begin{pmatrix} e^{-i\phi} \Phi'_1 \\ \Phi'_2 \\ e^{i\phi} \Phi'_3 \end{pmatrix}, \quad (8)$$

where Φ'_1, Φ'_2 and Φ'_3 are independent on ϕ . n is an integer number and characterizes phase winding. Three components carry phase winding $(n-1, n, n+1)$. There is a unit phase winding difference between them. With the help of $\bar{\Phi}$, the effective Hamiltonian H_{eff} can be diagonalized to get eigenvalues $E(n)$, from which we immediately realize that $E(n) = E(-n)$. Physically, the degeneracy of $E(n)$ and $E(-n)$ originates from the symmetry \hat{O} defined in Eq. (4). Therefore, the lowest energy state of the single-particle effective Hamiltonian H_{eff} is twofold degenerate.

The twofold degenerate lowest energy state offers an interesting accommodation for atoms to condense into. In the presence of the mean-field interactions, we construct the ground state ansatz by considering the superposition of the lowest energy state [38, 52],

$$\bar{\Phi}^{(\text{gs})} = C_+ \bar{\Phi}_n + C_- \hat{O} \bar{\Phi}_n. \quad (9)$$

Here,

$$\bar{\Phi}_n = e^{in\phi} \begin{pmatrix} e^{-i\phi} \cos \alpha \cos \beta \\ -\sin \alpha \\ e^{i\phi} \cos \alpha \sin \beta \end{pmatrix}, \quad (10)$$

which is an eigenstate of H_{eff} . The superposition coefficients C_+ and C_- satisfy $|C_+|^2 + |C_-|^2 = 1$. Substituting the trial wave function $\bar{\Phi}^{(\text{gs})}$ into the total energy E_{tot}

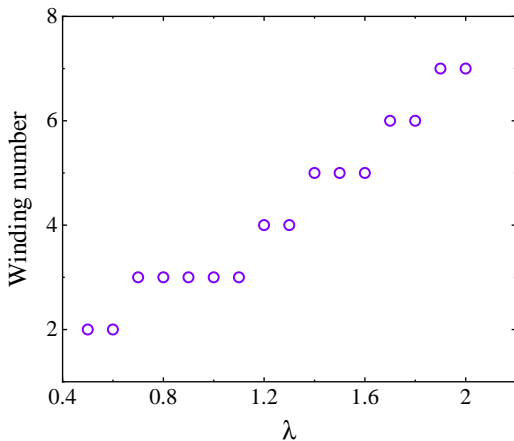


FIG. 4. The winding number of the second component as a function of λ . All parameters are same as in Fig. 3.

in Eq. (6), we get $E_{\text{tot}}(n, \alpha, \beta, C_+, C_-)$. All parameters n, α, β, C_+ and C_- , determining properties of the ground state, shall be fixed by minimizing the total energy E_{tot} .

According to the resulted parameters from the minimization, the ground state has the following phases:

(1) For antiferromagnetic interactions $\bar{c}_2 > 0$, there are two phases. We take $\bar{c}_0 = 10$ and $\bar{c}_2 = 1$ as an example. (I) When $\bar{\lambda} \leq 0.86$, the results are $n = 0$, $\beta = 3\pi/4$, and one of the C_+ and C_- is zero, i.e., $C_+ = 0, C_- = 1$, or $C_+ = 1, C_- = 0$. With these parameters, it can be seen that $\hat{O}\bar{\Phi}_{n=0} = -\bar{\Phi}_{n=0}$. $\bar{\Phi}_{n=0}$ and $\hat{O}\bar{\Phi}_{n=0}$ are a same state up to a sign difference. The ground state supports persistent flows. The phase winding of three components is always $-1, 0$ and 1 . $|\bar{\Phi}_1^{(\text{gs})}|^2 = |\bar{\Phi}_3^{(\text{gs})}|^2$, the size of which is always larger than that of $|\bar{\Phi}_2^{(\text{gs})}|^2$. This phase corresponds to the two dimensional analog as shown in Fig. 1(a). (II) When $\bar{\lambda} > 0.86$, results of the minimization are $n \neq 0$ and $C_+ = 1/\sqrt{2}, C_- = \pm 1/\sqrt{2}$. The ground state is the equal superposition of $\bar{\Phi}_n$ and $\hat{O}\bar{\Phi}_n$, and thus is an eigenstate of \hat{O} . Because of the superposition, the density of the ground state is periodically modulated along the azimuthal direction, $|\bar{\Phi}_1^{(\text{gs})}|^2 = |\bar{\Phi}_3^{(\text{gs})}|^2 = \cos^2 \alpha [1 \pm \sin(2\beta) \cos(2n\phi)]$, $|\bar{\Phi}_2^{(\text{gs})}|^2 = 2 \sin^2 \alpha [1 - \cos(2n\phi)]$, here \pm depends on the sign of C_- . Such density modulated ground states correspond to necklace states found in Fig. 1(b-d). The nature of necklace states is that the period of three components is same and is an even number $2n$.

(2) For ferromagnetic interactions $\bar{c}_2 < 0$, the minimization always chooses $C_+ = 0, C_- = 1$ or $C_+ = 1, C_- = 0$. The ground state is a persistent flow with phase winding number $(n-1, n, n+1)$ or $(-n-1, -n, -n+1)$ for three components. These two configurations are spontaneously chosen. The unique feature of such a ground state is that there is a unit phase winding difference between three components. These states correspond to two-dimensional persistent flows found in Fig. 3, where only

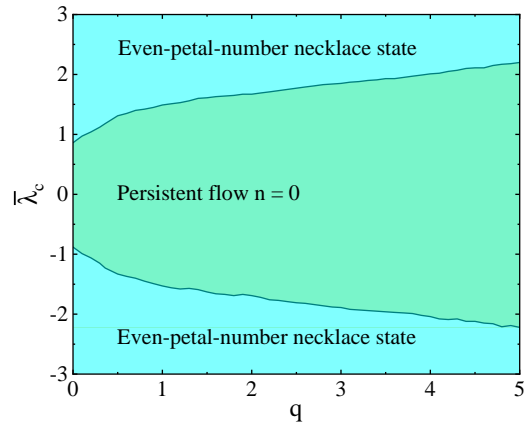


FIG. 5. The critical value of the spin-orbit coupling strength $\bar{\lambda}_c$ between the persistent flow and necklace state as a function of the quadratic Zeeman effect q for an antiferromagnetic interaction $\bar{c}_2 = 1$ from the one dimensional effective model. The other parameter is $\bar{c}_2 = 10$.

the configuration $(-n-1, -n, -n+1)$ is shown.

The possible existence of the even-petal-number necklace state in spin-1 BECs is due to the cooperation of symmetries \hat{O} and J_z . It is interesting to compare with a spin-1/2 system, where only the odd-petal-number state can exist. The effective azimuthal Hamiltonian for a Rashba coupled spin-1/2 is $H'_{\text{eff}} = (-i\partial/\partial\phi)^2 + \bar{\lambda}(\cos\phi\sigma_x + \sin\phi\sigma_y)(-i\partial/\partial\phi) - i\bar{\lambda}/2(\cos\phi\sigma_y - \sin\phi\sigma_x)$, which is similar as Eq. (5), but replacing spin-1 matrices F by spin-1/2 Pauli matrices σ [40, 43]. The conservation of $J'_z = -i\partial/\partial\phi + \sigma_z/2$ for H'_{eff} requires its eigenstates as $\bar{\Phi}'_n = e^{in\phi}(\Phi'_1, e^{i\phi}\Phi'_2)^T$. The symmetry $\hat{O}' = \mathcal{K}e^{i\pi\sigma_y/2}$ gives rise to the degeneracy of $\bar{\Phi}'_n$ and $\hat{O}'\bar{\Phi}'_n$. Therefore, the possible ground state is the superposition of $\bar{\Phi}'_n$ and $\hat{O}'\bar{\Phi}'_n$ with the corresponding density $\propto \cos[(2n+1)\phi]$. The necklace state in the spin-1/2 system takes odd petal-number. It is noting that there is a 1/2 in the symmetries \hat{O}' and J'_z , which is due to the $SU(2)$ nature of spin-1/2 spins. This unique $SU(2)$ property makes petal-number in necklace states of a spin-1/2 BEC odd.

We conclude that it is the symmetries \hat{O} and J_z of the Rashba spin-orbit coupling that leads to the existence of the persistent flow and necklace state. In spin-1 BECs, there is a unit phase winding difference between three components for persistent flows, and necklace states always have even petal-number.

At last, we would like to address the effect of the quadratic Zeeman coupling on above results. The quadratic Zeeman coupling plays an important role in spin-1 spinor BECs [47]. It is qF_z^2 , which should be incorporated into H_{sin} in Eq. (2) and H_{eff} in Eq. (5). Here, q describes the strength of the quadratic Zeeman term. In the Raman-induced spin-orbit-coupled spin-1 BEC experiment, it can be tuned [48]. It is interesting to find that the quadratic Zeeman term doesn't destroy the sym-

metries \hat{O} and J_z . Therefore, its existence doesn't quantitatively change the results from two-dimension numerical calculations and from the one-dimension analytical model. We find that it just slightly modifies the demarcation between the persistent flow and necklace state for antiferromagnetic interactions. In Fig. 5, we show the dependence of the critical spin-orbit coupling strength $\bar{\lambda}_c$ on the quadratic Zeeman effect q . For antiferromagnetic interactions, when $|\bar{\lambda}| < |\bar{\lambda}_c|$, the ground state is a persistent flow with $n = 0$ [see Eq. (10)], when $|\bar{\lambda}| > |\bar{\lambda}_c|$, the ground state is an even-petal-number necklace state. There is a slight increase of $|\bar{\lambda}_c|$ as a function of q . We also note that in Fig. 5 there is a symmetry between $\bar{\lambda} > 0$ and $\bar{\lambda} < 0$, this is because that the effective Hamiltonian $H_{\text{eff}} + qF_z^2$ has a spin rotation symmetry $e^{i\pi F_z}$, the physics in the $\bar{\lambda} < 0$ regime is the same as that in the regime of $\bar{\lambda} > 0$.

IV. CONCLUSION

We systematically study the ground-state phase diagram in a Rashba spin-orbit-coupled spin-1 BEC trapped in a two dimensional toroidal trap. The spin-flip symmetries of the spin-orbit coupling endow new features to the persistent flow and support the even-petal-number necklace state. The chosen phases depend on the sign of spinor's spin-spin interaction. The toroidal trapped spin-orbit-coupled BEC provides an experimentally accessible playground to investigate necklace states. They emerge as ground states with spontaneous breaking of the continuous rotation symmetry. Therefore, they are always dynamically unstable, which is in favor of experimental observation. The petal-number of the necklace state can be tuned by changing the spin-orbit coupling strength. The number is always odd in spin-1/2 BECs, while it is even in spin-1 systems.

ACKNOWLEDGMENTS

This work is supported by National Natural Science Foundation of China with Grants Nos. 11974235 and 11774219.

-
- [1] C. Ryu, M. F. Andersen, P. Cladé, V. Natarajan, K. Helmerson, and W. D. Phillips, Observation of persistent flow of a bose-einstein condensate in a toroidal trap, *Phys. Rev. Lett.* 99, 260401 (2007).
- [2] A. Ramanathan, K. C. Wright, S. R. Muniz, M. Zelan, W. T. Hill, C. J. Lobb, K. Helmerson, W. D. Phillips, and G. K. Campbell, Superflow in a toroidal bose-einstein condensate: An atom circuit with a tunable weak link, *Phys. Rev. Lett.* 106, 130401 (2011).
- [3] P. Mason and N. G. Berloff, Dynamics of quantum vortices in a toroidal trap, *Phys. Rev. A* 79, 043620 (2009).
- [4] A. V. Yulin, Y. V. Bludov, V. V. Konotop, V. Kuzmiak, and M. Salerno, Superfluidity of bose-einstein condensates in toroidal traps with nonlinear lattices, *Phys. Rev. A* 84, 063638 (2011).
- [5] S. Baharian and G. Baym, Bose-einstein condensates in toroidal traps: Instabilities, swallow-tail loops, and self-trapping, *Phys. Rev. A* 87, 013619 (2013).
- [6] A. Kumar, S. Eckel, F. Jendrzejewski, and G. K. Campbell, Temperature-induced decay of persistent currents in a superfluid ultracold gas, *Phys. Rev. A* 95, 021602 (2017).
- [7] J. Polo, R. Dubessy, P. Pedri, H. Perrin, and A. Minguzzi, Oscillations and decay of superfluid currents in a one-dimensional bose gas on a ring, *Phys. Rev. Lett.* 123, 195301 (2019).
- [8] M. Kunimi and I. Danshita, Decay mechanisms of superflow of bose-einstein condensates in ring traps, *Phys. Rev. A* 99, 043613 (2019).
- [9] S. Eckel, J. G. Lee, F. Jendrzejewski, N. Murray, C. W. Clark, C. J. Lobb, W. D. Phillips, M. Edwards, and G. K. Campbell, Hysteresis in a quantized superfluid 'atomtronic' circuit, *Nature* 506, 200 (2014).
- [10] A. Aftalion and P. Mason, Rotation of a bose-einstein condensate held under a toroidal trap, *Phys. Rev. A* 81, 023607 (2010).
- [11] R. Dubessy, T. Liennard, P. Pedri, and H. Perrin, Critical rotation of an annular superfluid bose-einstein condensate, *Phys. Rev. A* 86, 011602 (2012).
- [12] A. White, T. Hennessy, and T. Busch, Emergence of classical rotation in superfluid bose-einstein condensates, *Phys. Rev. A* 93, 033601 (2016).
- [13] A. Roussou, J. Smyrnakis, M. Magiropoulos, N. K. Efremidis, and G. M. Kavoulakis, Rotating bose-einstein condensates with a finite number of atoms confined in a ring potential: Spontaneous symmetry breaking beyond the mean-field approximation, *Phys. Rev. A* 95, 033606 (2017).
- [14] A. Muñoz Mateo, V. Delgado, M. Guilleumas, R. Mayol, and J. Brand, Nonlinear waves of bose-einstein condensates in rotating ring-lattice potentials, *Phys. Rev. A* 99, 023630 (2019).
- [15] A. Pérez-Obiol and T. Cheon, Bose-einstein condensate confined in a one-dimensional ring stirred with a rotating delta link, *Phys. Rev. E* 101, 022212 (2020).
- [16] B. Eller, O. Oladehin, D. Fogarty, C. Heller, C. W. Clark, and M. Edwards, Producing flow in racetrack atom circuits by stirring, *Phys. Rev. A* 102, 063324 (2020).
- [17] E. Arabahmadi, D. Schumayer, and D. A. W. Hutchinson, Universal nomogram for the atomtronic quantum rotation sensor, *Phys. Rev. A* 103, 043319 (2021).
- [18] S. Beattie, S. Moulder, R. J. Fletcher, and Z. Hadzibabic, Persistent currents in spinor condensates, *Phys. Rev. Lett.* 110, 025301 (2013).

- [19] J. Smyrnakis, S. Bargi, G. M. Kavoulakis, M. Magiropoulos, K. Kärkkäinen, and S. M. Reimann, Mixtures of bose gases confined in a ring potential, *Phys. Rev. Lett.* 103, 100404 (2009).
- [20] S. Bargi, F. Malet, G. M. Kavoulakis, and S. M. Reimann, Persistent currents in bose gases confined in annular traps, *Phys. Rev. A* 82, 043631 (2010).
- [21] K. Anoshkin, Z. Wu, and E. Zaremba, Persistent currents in a bosonic mixture in the ring geometry, *Phys. Rev. A* 88, 013609 (2013).
- [22] M. Abad, A. Sartori, S. Finazzi, and A. Recati, Persistent currents in two-component condensates in a toroidal trap, *Phys. Rev. A* 89, 053602 (2014).
- [23] T. Shimodaira, T. Kishimoto, and H. Saito, Connection between rotation and miscibility in a two-component bose-einstein condensate, *Phys. Rev. A* 82, 013647 (2010).
- [24] Z. Wu, E. Zaremba, J. Smyrnakis, M. Magiropoulos, N. K. Efremidis, and G. M. Kavoulakis, Mean-field yrast spectrum and persistent currents in a two-component bose gas with interaction asymmetry, *Phys. Rev. A* 92, 033630 (2015).
- [25] Z. Chen, Y. Li, N. P. Proukakis, and B. A. Malomed, Immiscible and miscible states in binary condensates in the ring geometry, *New J. Phys.* 21, 073058 (2019).
- [26] A. Roussou, J. Smyrnakis, M. Magiropoulos, N. K. Efremidis, G. M. Kavoulakis, P. Sandin, M. Ögren, and M. Gulliksson, Excitation spectrum of a mixture of two bose gases confined in a ring potential with interaction asymmetry, *New J. Phys.* 20, 045006 (2018).
- [27] H. Mäkelä and E. Lundh, Excitation spectrum of a toroidal spin-1 bose-einstein condensate, *Phys. Rev. A* 88, 033622 (2013).
- [28] A. I. Yakimenko, K. O. Isaieva, S. I. Vilchinskii, and M. Weyrauch, Stability of persistent currents in spinor bose-einstein condensates, *Phys. Rev. A* 88, 051602 (2013).
- [29] M. Kunimi, Metastable spin textures and nambu-goldstone modes of a ferromagnetic spin-1 bose-einstein condensate confined in a ring trap, *Phys. Rev. A* 90, 063632 (2014).
- [30] D. L. Campbell, G. Juzeliūnas, and I. B. Spielman, Realistic rashba and dresselhaus spin-orbit coupling for neutral atoms, *Phys. Rev. A* 84, 025602 (2011).
- [31] Y. J. Lin, K. Jiménez-García, and I. B. Spielman, Spin-orbit-coupled bose-einstein condensates, *Nature* 471, 83 (2011).
- [32] Z. Wu, L. Zhang, W. Sun, X.-T. Xu, B.-Z. Wang, S.-C. Ji, Y. Deng, S. Chen, X.-J. Liu, and J.-W. Pan, Realization of two-dimensional spin-orbit coupling for bose-einstein condensates, *Science* 354, 83 (2016).
- [33] C. Hamner, Y. Zhang, M. A. Khamahchi, M. J. Davis, and P. Engels, Spin-orbit-coupled bose-einstein condensates in a one-dimensional optical lattice, *Phys. Rev. Lett.* 114, 070401 (2015).
- [34] C. Wang, C. Gao, C.-M. Jian, and H. Zhai, Spin-orbit coupled spinor bose-einstein condensates, *Phys. Rev. Lett.* 105, 160403 (2010).
- [35] T.-L. Ho and S. Zhang, Bose-einstein condensates with spin-orbit interaction, *Phys. Rev. Lett.* 107, 150403 (2011).
- [36] H. Hu, B. Ramachandhran, H. Pu, and X.-J. Liu, Spin-orbit coupled weakly interacting bose-einstein condensates in harmonic traps, *Phys. Rev. Lett.* 108, 010402 (2012).
- [37] Y. Zhang, L. Mao, and C. Zhang, Mean-field dynamics of spin-orbit coupled bose-einstein condensates, *Phys. Rev. Lett.* 108, 035302 (2012).
- [38] Y. Li, L. P. Pitaevskii, and S. Stringari, Quantum tricriticality and phase transitions in spin-orbit coupled bose-einstein condensates, *Phys. Rev. Lett.* 108, 225301 (2012).
- [39] J.-R. Li, J. Lee, W. Huang, S. Burchesky, B. Shteynas, F. C. Top, A. O. Jamison, and W. Ketterle, A stripe phase with supersolid properties in spin-orbit-coupled bose-einstein condensates, *Nature* 543, 91 (2017).
- [40] O. Fialko, J. Brand, and U. Zülicke, Soliton magnetization dynamics in spin-orbit-coupled bose-einstein condensates, *Phys. Rev. A* 85, 051605 (2012).
- [41] E. O. Karabulut, F. Malet, A. L. Fetter, G. M. Kavoulakis, and S. M. Reimann, Spin-orbit-coupled bose-einstein-condensed atoms confined in annular potentials, *New J. Phys.* 18, 015013 (2016).
- [42] X.-F. Zhang, M. Kato, W. Han, S.-G. Zhang, and H. Saito, Spin-orbit-coupled bose-einstein condensates held under a toroidal trap, *Phys. Rev. A* 95, 033620 (2017).
- [43] A. C. White, Y. Zhang, and T. Busch, Odd-petal-number states and persistent flows in spin-orbit-coupled bose-einstein condensates, *Phys. Rev. A* 95, 041604 (2017).
- [44] J.-G. Wang, L.-L. Xu, and S.-J. Yang, Ground-state phases of the spin-orbit-coupled spin-1 bose gas in a toroidal trap, *Phys. Rev. A* 96, 033629 (2017).
- [45] H. Wang, L. Wen, H. Yang, C. Shi, and J. Li, Vortex states and spin textures of rotating spin-orbit-coupled bose-einstein condensates in a toroidal trap, *Journal of Physics B: Atomic, Molecular and Optical Physics* 50, 155301 (2017).
- [46] P. Peng, G.-Q. Li, W.-L. Yang, and Z.-Y. Yang, Exotic ground states of a spin-orbit-coupled spinor bose-einstein condensate trapped by a toroidal potential, *Laser Physics Letters* 15, 085501 (2018).
- [47] Y. Kawaguchi and M. Ueda, Spinor bose-einstein condensates, *Physics Reports* 520, 253 (2012).
- [48] D. L. Campbell, A. Price, R. M. and Putra, A. ValdésCurie, D. Trypogeorgos, and I. B. Spielman, Magnetic phases of spin-1 spin-orbit-coupled bose gases, *Nat. Commun.* 7, 10897 (2016).
- [49] Z. Lan and P. Öhberg, Raman-dressed spin-1 spin-orbit-coupled quantum gas, *Phys. Rev. A* 89, 023630 (2014).
- [50] S. S. Natu, X. Li, and W. S. Cole, Striped ferronematic ground states in a spin-orbit-coupled $s = 1$ bose gas, *Phys. Rev. A* 91, 023608 (2015).
- [51] Z.-Q. Yu, Phase transitions and elementary excitations in spin-1 bose gases with raman-induced spin-orbit coupling, *Phys. Rev. A* 93, 033648 (2016).
- [52] K. Sun, C. Qu, Y. Xu, Y. Zhang, and C. Zhang, Interacting spin-orbit-coupled spin-1 bose-einstein condensates, *Phys. Rev. A* 93, 023615 (2016).
- [53] G. I. Martone, F. V. Pepe, P. Facchi, S. Pascazio, and S. Stringari, Tricriticalities and quantum phases in spin-orbit-coupled spin-1 bose gases, *Phys. Rev. Lett.* 117, 125301 (2016).
- [54] F. E. Meijer, A. F. Morpurgo, and T. M. Klapwijk, One-dimensional ring in the presence of rashba spin-orbit interaction: Derivation of the correct hamiltonian, *Phys. Rev. B* 66, 033107 (2002).